PNAS RESEARCH ARTICLE | CELL BIOLOGY

Cellular redox homeostasis maintained by malic enzyme 2 is essential for MYC-driven T cell lymphomagenesis

Wei Li[a,1], Junjie Kou[a,1], Zhenxi Zhang[a], Haoyue Li[a], Li Li[a], and Wenjing Du[a,2]

Edited by Karen Vousden, The Francis Crick Institute, London, United Kingdom; received October 19, 2022; accepted April 28, 2023

T cell lymphomas (TCLs) are a group of rare and heterogeneous tumors. Although proto-oncogene *MYC* has an important role in driving T cell lymphomagenesis, whether MYC carries out this function remains poorly understood. Here, we show that malic enzyme 2 (ME2), one of the NADPH-producing enzymes associated with glutamine metabolism, is essential for MYC-driven T cell lymphomagenesis. We establish a *CD4-Cre; Myc*$^{flox/+}$ transgenic mouse mode, and approximately 90% of these mice develop TCL. Interestingly, knockout of *Me2* in *Myc* transgenic mice almost completely suppresses T cell lymphomagenesis. Mechanistically, by transcriptionally up-regulating ME2, MYC maintains redox homeostasis, thereby increasing its tumorigenicity. Reciprocally, ME2 promotes MYC translation by stimulating mTORC1 activity through adjusting glutamine metabolism. Treatment with rapamycin, an inhibitor of mTORC1, blocks the development of TCL both in vitro and in vivo. Therefore, our findings identify an important role for ME2 in MYC-driven T cell lymphomagenesis and reveal that MYC–ME2 circuit may be an effective target for TCL therapy.

malic enzyme 2 | glutamine metabolism | redox homeostasis | MYC | T cell lymphomas

T cell lymphomas (TCLs) are a group of biologically and clinically heterogeneous lymphoblastic tumors (1). T cells acquire various genetic aberrations during and/or after maturation, leading to the development of T-lymphoblastic malignancies (2). Although novel chemotherapy, targeted therapy, or immunotherapy have revolutionized the treatment of human lymphoma, the overall prognosis for patients with TCL is inferior to that of B cell lymphoma, and the survival rate for patients with relapsed TCL remains low (3). Indeed, the rarity and heterogeneity of TCL pose several challenges to the research and treatment of the disease (4). Further exploration to understand the biology of these tumors is expected to change patient outcomes.

MYC acts as a transcription factor that regulates a range of target genes to exert their biological effects, including cell growth and proliferation, cell cycle, apoptosis, and nutrient metabolism (5). The expression of MYC is frequently dysregulated and enhanced in many human tumor types due to chromosomal translocations, copy number changes, or being downstream of multiple oncogenic signaling pathways (6–8). Indeed, MYC is critical to the development of a large proportion of TCL patients. Tissue microarrays from 1,214 lymphomas showed that 94% of TCL samples were positive for MYC staining (9). *MYC* rarely exhibits rearrangement in TCL, but it is frequently overexpressed through multiple signaling pathways, leading to the development of this disease (10, 11). Studies on transgenic mice provide evidence of a critical role for MYC in tumorigenesis. For example, *Eμ-Myc* mice that mimic the chromosomal translocation of Burkitt lymphoma fully develop B cell lymphoma (12). For TCL, constitutive overexpression of MYC in mouse or zebrafish T-lineage cells leads to T cell lymphomagenesis (13–15). Conversely, depletion of MYC expression inhibits TCL development both in vitro and in vivo (11, 16), indicating the important role for MYC in TCL progression. However, it remains unclear how MYC reprograms cells to promote T cell lymphomagenesis.

Malic enzymes are $NADP^+$ (NAD^+)-dependent enzymes, which link glutamine and glucose metabolism through oxidizing malate to pyruvate and NADPH (NADH). There are three isoforms of malic enzymes in mammalian cells (17–19). As the major isoform of malic enzymes, ME2 plays important role in cell senescence, NADPH production, and lipogenesis through adjusting glutaminolysis (20–22). In addition to this, recent studies have revealed the distinct mechanism by which ME2 promotes cell proliferation in different cells. For instance, ME2 promotes osteoblast proliferation and differentiation by maintaining glycolytic flux (23). In addition, ME2 supports cell growth through regulating mitochondrial biomass production independent of its catalytic activity in acute myeloid leukemia (AML) (24). Interestingly, our recent study identified a noncanonical physiological function of ME2 in producing 2-hydroxygluatrate (2-HG), which stabilizes mutant p53 protein that contributes to tumor growth (25).

Significance

The overall prognosis for T cell lymphoma (TCL) patients remains poor due to the rarity and heterogeneity of this disease. Oncogenic transcription factor MYC is critical to the development of a large proportion of TCL patients. Constitutive MYC overexpression leads to TCL tumor initiation and progression, while MYC depletion slows down tumor growth. However, it remains unclear how MYC functions to promote T cell lymphomagenesis. We report here that malic enzyme 2 (ME2) promotes MYC-driven T cell lymphomagenesis by maintaining redox homeostasis. Breaking MYC–ME2 circuit with rapamycin alleviates TCL progression in patients with high MYC expression.

Author affiliations: [a]State Key Laboratory of Medical Molecular Biology, Haihe Laboratory of Cell Ecosystem, Department of Cell Biology, Institute of Basic Medical Sciences Chinese Academy of Medical Sciences, School of Basic Medicine Peking Union Medical College 100005, Beijing, China

Author contributions: W.L. and W.D. designed research; W.L. and J.K. performed research; W.L., Z.Z., and W.D. analyzed data; H.L. and L.L. provided technical assistance; and W.D. wrote the paper.

The authors declare no competing interest.

This article is a PNAS Direct Submission.

[1]W.L. and J.K. contributed equally to this work.

[2]To whom correspondence may be addressed. Email: wenjingdu@ibms.pumc.edu.cn.

This article contains supporting information online at https://www.pnas.org/lookup/suppl/doi:10.1073/pnas.2217869120/-/DCSupplemental.

Published May 30, 2023.

We previously found that p53 inhibits ME2 including ME1 transcription, and reciprocally, ME1 and ME2 inhibit p53 activation through different mechanisms (21). A recent study reported an important role for ME1 in the regulation of redox homeostasis in synovial sarcoma (26). Here, we report that ME2 is a target of MYC and plays a critical role in MYC-driven T cell lymphomagenesis. We establish a T cell lymphoma mouse model by constitutively overexpressing MYC in T-lineage cells under the control of *CD4* promoter. This model provides additional evidence for the critical status of MYC in T cell lymphomagenesis. Interestingly, knockout *Me2* in these mice completely suppresses tumorigenesis, indicating an essential role of ME2 in MYC-induced T cell lymphomagenesis. Mechanistically, MYC maintains intracellular redox homeostasis via ME2-mediated glutamine metabolism, thereby promoting T cell lymphomagenesis. Importantly, we further reveal a positive feedback loop between ME2 and MYC in glutamine metabolism and redox maintenance in TCL. Breaking this feedback loop by targeting mTORC1 pathway effectively alleviates TCL progression. Our findings uncover the important status of ME2 in MYC-induced TCL and may provide unique strategies for TCL treatment.

Results

ME2 Is Required for the Progression of T Cell Lymphoma. To investigate the function of malic enzymes in TCL, we analyzed the expression of three isoforms of malic enzymes in 13 TCL cell lines derived from Cancer Cell Line Encyclopedia (CCLE) database (https://portals.broadinstitute.org/ccle). *ME2* expression levels were relatively higher than *ME1* and *ME3* in these cell lines (*SI Appendix*, Fig. S1*A*). Analysis of 61 human lymphoma cell lines also confirmed this observation (*SI Appendix*, Fig. S1 *A* and *B*). We further analyzed several publicly available human T cell lymphoma databases from Gene Expression Omnibus (GEO) (GSE132053, GSE168508, GSE58445) and identified that the expression of *ME2* was much higher than that of *ME1* and *ME3* (*SI Appendix*, Fig. S1 *C*–*E*). In addition, we analyzed *ME2* expression in 1,035 human cancer cell lines and found that, unlike other cancer cell lines, *ME2* was most highly expressed in hematopoietic and lymphatic cancers, while *ME1* and *ME3* were rarely expressed (*SI Appendix*, Fig. S1*F*). Moreover, a survey from GEO showed that *ME2* expression, but not *ME1* or *ME3*, was significantly up-regulated in mouse TCL tissues compared with normal lymphoid tissues (*SI Appendix*, Fig. S1*G*). Next, we examined ME expression by immunohistochemistry staining (IHC) of tumor microarrays containing 52 human TCL tissues and 8 normal lymphoid tissues. ME2 expression was generally up-regulated in TCL samples, while ME1 and ME3 was not (Fig. 1*A*). In addition, the expression of *ME1* and *ME3* was very low and hard to detect in two TCL cell lines, Jurkat and MOLT4 (*SI Appendix*, Fig. S1*H*). These data indicate that ME2, rather than ME1 and ME3, plays an important role in T cell lymphomagenesis.

To investigate whether ME2 is required for TCL's cell proliferation in vitro, we stably knocked down *ME2* with short hairpin RNA (shRNA) in two TCL cell lines Jurkat and MOLT4. *ME2* knockdown was confirmed by western blot and enzymatic activity measurement (Fig. 1*B* and *SI Appendix*, Fig. S1 *I*, *Left*). Suppression of *ME2* inhibited cell proliferation in both Jurkat cells and MOLT4 cells (Fig. 1*B* and *SI Appendix*, Fig. S1 *I*, *Right*). However, *ME2* depletion had no effect on cell apoptosis (Fig. 1*C* and *SI Appendix*, Fig. S1*J*). In a soft agar assay, Jurkat cells deprived of *ME2* expression reduced the anchorage-independent colony formation (Fig. 1*D*). Similar results were obtained in MOLT4 cells (*SI Appendix*, Fig. S1*K*). Conversely, overexpression of *ME2* enhanced cell proliferation in both Jurkat and MOLT4 cells, along with increased intracellular ME2 expression and enzymatic activity (Fig. 1*E* and *SI Appendix*, Fig. S1*L*). Consistently, cells stably expressing *ME2* showed increased anchorage-independent growth (Fig. 1*F* and *SI Appendix*, Fig. S1*M*). To exclude the off-target effect of shRNA, we performed a rescue experiment using shRNA-resistant *ME2* cDNA. As shown in *SI Appendix*, Fig. S1*N*, enforced expression of exogenous *ME2* rescued the expression and enzymatic activity of ME2 and restored the cell proliferation in *ME2*-depleted cells.

Next, we investigated whether ME2 impairs TCL progression in vivo. We injected Jurkat cells stably expressing control or *ME2* shRNA into immunocompromised NSG mice, a well-established TCL model to mimic disease development in the circulatory system (27). The overall survival of the mice bearing *ME2*-depleted cells was much longer than the mice bearing control cells, which all died within 35 d (Fig. 1*G*). Meanwhile, mice bearing *ME2*-depleted cells showed less dispersion of human $CD45^+$ cells in the bone marrow, blood, and spleens (*SI Appendix*, Fig. S1*O*) and manifested more reddish bones (*SI Appendix*, Fig. S1*P*) and decreased spleen weight (Fig. 1*H*). More reddish bones implied that less proliferation of Jurkat cells in mice bearing *ME2*-depleted cells compared to the mice bearing control cells (*SI Appendix*, Fig. S1*P*). Moreover, IHC staining showed a decrease in TCL burden and reduced proliferation in the spleens from the mice carrying *ME2* knocked down cells (*SI Appendix*, Fig. S1*Q*). Taken together, these data suggest that ME2 is essential for TCL progression both in vitro and in vivo.

ME2 Is a Target Gene for MYC. MYC is frequently up-regulated by multiple deregulated pathways in TCL (10, 11). We analyzed the CCLE database and found that mRNA expression of *MYC* was positively correlated with *ME*2 in 13 TCL cell lines (Fig. 2*A*). IHC staining of tumor microarrays containing 52 human TCL samples showed that the protein expression level of MYC was also positively correlated with ME2 (Fig. 2*B*). In keeping with the finding of low expression of ME1 and ME3 in TCL, there was no correlation between MYC and ME1 or ME3 (Fig. 2 *C* and *D*). In addition, mRNA expression of *MYC* was positively correlated with *ME2* in thymoma, lymphoid neoplasm diffuse large B cell lymphoma, cholangiocarcinoma, and thyroid carcinoma, from the Cancer Genome Atlas database (*SI Appendix*, Fig. S2*A*). Knockdown of MYC resulted in a reduction in protein and mRNA levels of ME2 in the human B lymphocyte cell line Ramos and Raji, the human CHOL cell line RBE, and the human thyroid cancer cell line SW579 (*SI Appendix*, Fig. S2*B*), suggesting that MYC may regulate ME2 expression. In Jurkat and MOLT4 cells, *MYC* knockdown led to a noticeable decline in both the enzymatic activity and expression levels of ME2 (Fig. 2*E* and *SI Appendix*, Fig. S2*C*). To exclude the off-target effect of shRNA, we performed a rescue experiment using shRNA-resistant *MYC* cDNA. Enforced expression of exogenous MYC in *MYC* knockdown cells restored ME2 expression in both mRNA and protein levels (*SI Appendix*, Fig. S2*D*). Additionally, inhibition of *MYC* by two different sets of siRNAs reduced ME2 activity and expression in both cell lines (*SI Appendix*, Fig. S2 *E* and *F*). Conversely, enforced expression of MYC augmented both the activity and expression of ME2 (Fig. 2*F* and *SI Appendix*, Fig. S2*G*). Besides, JQ1 is a selective inhibitor of BET bromodomain that restrains *MYC* transcription (28). When cells were treated with JQ1, MYC expression was inhibited, leading to a reduction in both ME2 activity and expression (*SI Appendix*, Fig. S2 *H* and *I*). These results indicate that MYC enhances the expression of ME2.

To further evaluate the upregulation of ME2 by MYC in vivo, we generated *CD4-Cre; Myc*$^{flox/+}$ (*Myc* transgenic, *Myc*Tg) mice,

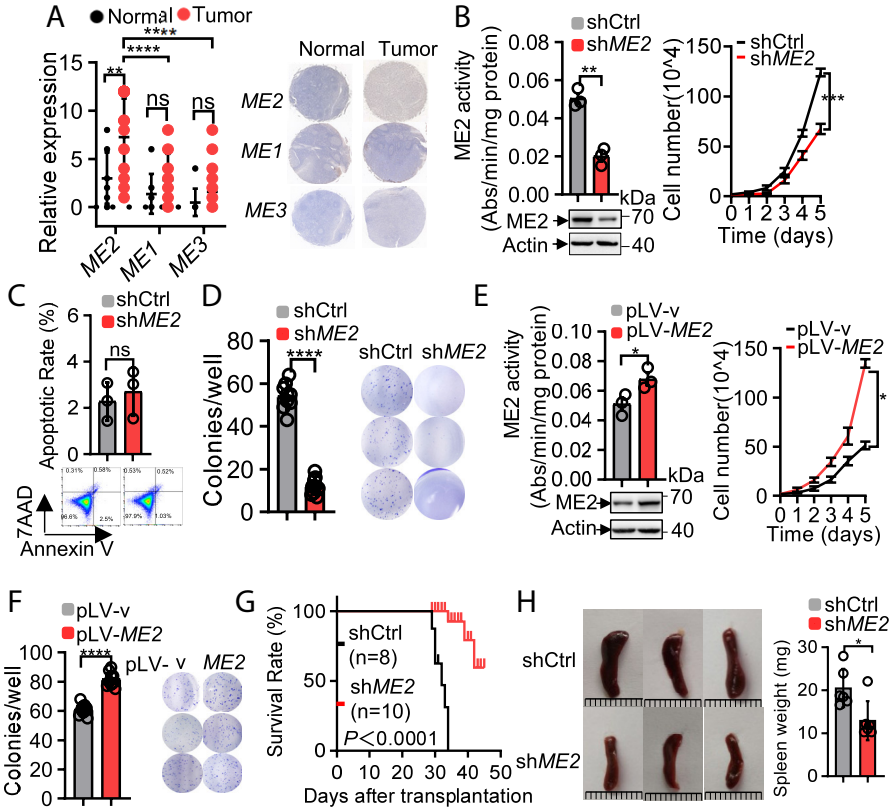

Fig. 1. ME2 is essential for TCL cell growth both in vitro and in vivo. (*A*) Paraffin sections of human TCL microarrays analyzed by immunohistochemistry. Expression score of ME2, ME1, and ME3 in human TCL samples (n = 52) compared with normal samples (n = 8) (*Left*). Expression score was determined by staining scope and staining intensity. Representative pictures are shown (*Right*). (*B–D*) Jurkat cells were infected with lentiviruses expressing control or *ME2* shRNA. (*B*) ME2 enzymatic activity (*Left Top*), protein levels (*Left Bottom*), and cell proliferation (*Right*) were examined. (*C*) Cell apoptosis was analyzed by flow cytometry (*Bottom*) and quantified (*Top*). (*D*) Cells were plated in culture medium in soft agar. Colonies were stained with crystal violet at day 20. Numbers of colonies with a diameter greater than 20 μm were quantified (*Left*). Representative images of colonies in soft agar are shown (*Right*). (*E* and *F*) Jurkat cells were infected with lentiviruses overexpressing *ME2* or empty vector. (*E*) ME2 enzymatic activity (*Left Top*), protein levels (*Left Bottom*), and cell proliferation (*Right*) were examined. (*F*) Cells were plated in culture medium in soft agar. Colonies were stained with crystal violet at day 20. Numbers of colonies with a diameter greater than 20 μm were quantified (*Left*). Representative images of colonies in soft agar are shown (*Right*). (*G* and *H*) Jurkat cells stably infected with lentiviruses expressing control or *ME2* shRNA were injected into NSG mice. The mice were analyzed 4 wk later. (*G*) Kaplan–Meier survival curves of mice in two groups are shown. (*H*) Representative images of spleens (*Left*) in NSG mice carrying sh*ME2* or control Jurkat cells on day 28 post transplantation. Spleen weight was quantified (*Right*). Data in (*B–F*) are from n = 3 biological replicates. Data in (*G* and *H*) are from n = 6 biological replicates. Data are the mean ± SD. Statistical significance was determined by two-tailed unpaired *t* test. For *G*, statistical significance was calculated using log-rank analysis. *$P < 0.05$, **$P < 0.01$; ***$P < 0.001$; ****$P < 0.0001$; ns $P > 0.05$.

leading to heterozygous overexpression of *Myc* at the $CD4^+CD8^+$ double-positive (DP) stage of developing T-thymocytes (*SI Appendix*, Fig. S3*A*). *Myc* was excessively expressed in both thymuses and spleens (Fig. 2 *G* and *H*). Accordingly, both mRNA and protein levels of ME2 were higher in these tissues from *Myc*Tg mice when compared with wild-type mice (Fig. 2 *G* and *H*). These mice initially showed no thymic hyperplasia (*SI Appendix*, Fig. S5 *A*, *Left*), but subsequently developed locally invasive T cell lymphomas, leading to premature death within 100 to 420 d (Fig. 3*I* and *SI Appendix*, Table S1). We analyzed the mRNA levels of *ME2* and *MYC* in these lymphomas from *Myc*Tg mice. The expression of *ME2* showed a high positive correlation with *MYC* (Fig. 2*I*). Taken together, these data demonstrate that MYC enhances ME2 expression both in vitro and in vivo.

To determine whether MYC is a transcriptional activator for the *ME2* gene, we analyzed the *ME2* gene sequence for potential MYC response elements, which share the consensus E-box sequence of 5′-CACGTG-3′. Two potential response elements (*RE1* and *RE2*) were identified within the promoter region of *ME2* gene (*SI Appendix*, Fig. S3*B*). To investigate the binding of MYC to these two response elements, we performed chromatin immunoprecipitation (ChIP)-quantitative PCR (ChIP-qPCR) assay in Jurkat and MOLT4 cell lines. MYC bound to the potential response elements *RE1* and *RE2* of *ME2* as well as the response element of *LDHA* (*LDHA*-RE), which is a well-known target gene of MYC as a positive control (*SI Appendix*, Fig. S3*C*). To evaluate whether the response elements (*RE1* and *RE2*) within *ME2* confer MYC-dependent transcriptional activation, we cloned DNA fragments containing the wild-type or mutant response elements into the promoter region of a firefly luciferase reporter plasmid. MYC was able to induce luciferase expression from the wild-type reporter plasmids but not from the mutant reporter plasmids (*SI Appendix*, Fig. S3*D*). To activate transcription, MYC interacts with the small bHLHZ protein MAX to form heterodimer and binds to specific DNA (29). In the absence of MAX, MYC failed to activate the wild-type *RE*-responsive luciferase (*SI Appendix*, Fig. S3*E*), suggesting that MYC–MAX heterodimer is required for the transcription of *ME2*. Moreover, *MYC* contains several evolutionarily conserved transactivation domains, of which the deletion of MYC homology boxes II (*MBII*) dramatically reduces the transactivation function of MYC (30). Correspondingly, MYC without MBII domain was unable to induce the wild-type *RE*-responsive luciferase expression (*SI Appendix*, Fig. S3*F*). Taken together, these results reveal that ME2 is a MYC transcriptional target.

ME2 Is Essential for MYC-Mediated T Cell Lymphomagenesis. We next examined the role of ME2 in MYC-mediated TCL cell growth. Knockdown of *MYC* reduced cell proliferation in both

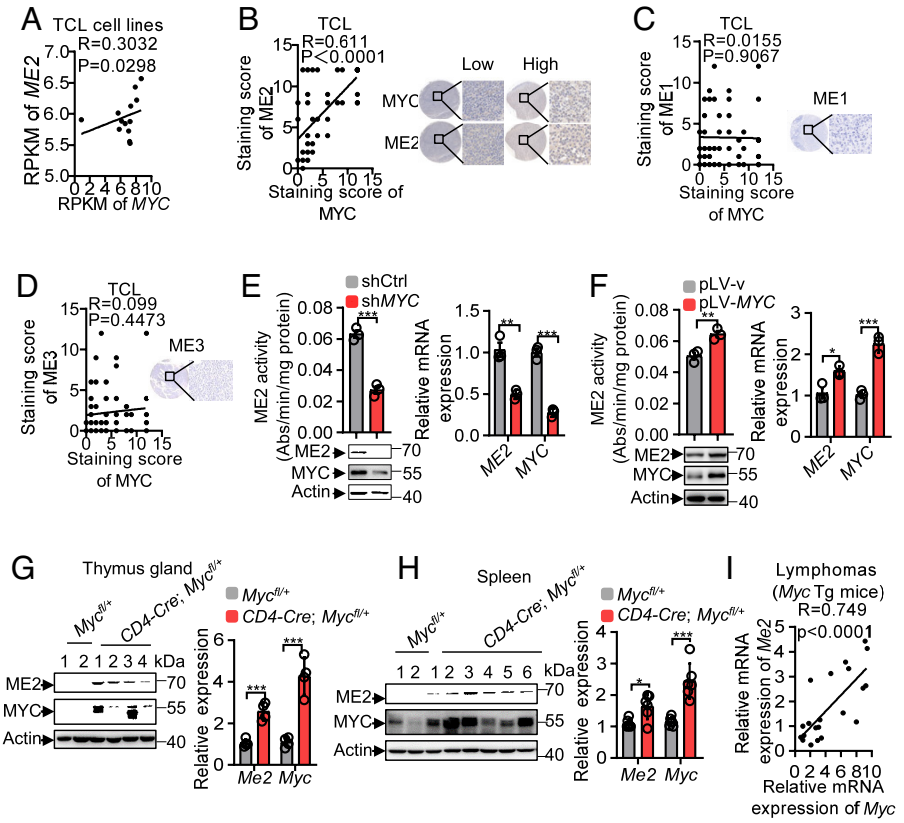

Fig. 2. MYC transcriptionally up-regulates ME2 expression. (*A*) Positive correlation between *ME2* and *MYC* mRNA levels in 13 human TCL cell lines from CCLE database. mRNA levels were presented as RPKM. Pearson's correlation coefficient (R) is shown. (*B–D*) Correlation between ME2 (*B*)/ME1 (*C*)/ME3 (*D*) and MYC immunohistochemical scores in human TCL microarrays (n = 52) (*Left*). Pearson's correlation coefficient (R) is shown. Representative images of tumor microarrays are shown (*Right*). (*E*) Jurkat cells were infected with lentiviruses expressing control or *MYC* shRNA. ME2 enzymatic activity (*Left Top*), protein expression (*Left Bottom*), and mRNA levels (*Right*) were examined. (*F*) Jurkat cells were infected with lentiviruses overexpressing *MYC* or empty vector. ME2 enzymatic activity (*Left Top*), protein expression (*Left Bottom*), and mRNA levels (*Right*) were examined. (*G* and *H*) Protein (*Left*) and mRNA (*Right*) levels of ME2 and MYC in the thymus gland (*G*) and spleen tissues (*H*) from $Myc^{fl/+}$ and *CD4-Cre;* $Myc^{fl/+}$ transgenic mice. (*I*) Positive correlation of *Me2* and *Myc* mRNA levels in TCL tissues (n = 22) from *CD4-Cre;* $Myc^{fl/+}$ transgenic mice. Pearson's correlation coefficient (R) is shown. Data in (*E* and *F*) are from n = 3 biological replicates. Data in (*G*) are from n = 4 biological replicates. Data in *H* are from n = 6 biological replicates. Data are the mean ± SD. Statistical significance was determined by two-tailed unpaired *t* test. **P* < 0.05, ***P* < 0.01; ****P* < 0.001; *****P* < 0.0001; ns *P* > 0.05.

Jurkat and MOLT4 cells, while enforced expression of *ME2* almost completely restored the proliferation of *MYC* knockdown cells (*SI Appendix*, Fig. S4 *A* and *B*). In a soft agar assay, cells stably expressing *ME2* showed enhanced anchorage-independent growth in control cells and especially in *MYC*-depleted cells (*SI Appendix*, Fig.S4 *C* and *D*). Likewise, overexpression of *ME2* restored both cell proliferation and anchorage-independent growth in JQ1-treated Jurkat and MOLT4 cells (*SI Appendix*, Fig.S4 *E–H*). These results suggest that MYC plays a role in promoting TCL cell growth, and this effect of MYC is mediated, at least in part, by ME2. To determine whether the effect of ME2 is due to its enzymatic activity, we generated a ME2 mutation (ME2 mut), which exhibited no enzymatic activity (21). In agreement with previous findings, knockdown of *MYC* reduced ME2 enzymatic activity, and reintroduction of wild-type ME2, but not mutant ME2 (mut), restored cellular ME2 enzymatic activity (*SI Appendix*, Fig. S4 *I* and *J*). Consistent with cellular ME2 activity, ectopic expression of wild-type ME2, but not mutant ME2, accelerated the growth of *MYC* knockdown cells (*SI Appendix*, Fig. S4 *K* and *L*). Similarly, only wild-type ME2 restored anchorage-independent growth of *MYC* knockdown cells (*SI Appendix*, Fig. S4 *M* and *N*). These results indicate that ME2 is required for MYC-mediated TCL cell growth, which depends on its enzymatic activity.

To explore whether ME2 expression is essential for the tumorigenesis of MYC-induced TCL in vivo, we established the *Myc*-constitutively overexpressed mouse model under the control of *CD4* promoter (*Myc*Tg mice) as shown in *SI Appendix*, Fig. S3*A*. We first investigated T cell development in *Myc*Tg mice. *Myc*Tg mice were born alive and appeared to be healthy. At approximately 6 to 8 wk of age, *Myc*Tg mice had normal thymus weight, spleen weight, and white cell differential counts in peripheral blood compared with wild-type control mice (*SI Appendix*, Fig. S5*A*). Flow cytometric analysis exhibited that *Myc*Tg mice had normal T cell subpopulation of thymocytes and peripheral T cells compared with wild-type control mice (*SI Appendix*, Fig. S5 *B* and *C*), suggesting that MYC overexpression has no effect on T cell development. *Myc*Tg mice developed neoplasms in different parts of the body, with approximately 90% of mice developing neoplasms in the lungs, 55% in the tail, and 10% in the thymus or legs (Fig. 3 *A* and *B*). Nevertheless, the white cell counts in peripheral blood from *Myc*Tg mice did not differ from those in wild-type mice at the age of 2 mo, 4 mo, and 6 mo (*SI Appendix*, Fig. S5*D*). Moreover, detailed immunophenotypic analysis of these neoplasms which developed in *Myc*Tg mice showed that they were a highly heterogeneous group of tumors showing distinct CD4 and CD8 cell surface expression patterns (Fig. 3*C*). And CD3 and CD19 staining suggested that these tumors were derived from T cell lineage rather than B cell lineage (Fig. 3*C*). The detailed information for the lymphomas of tumor-bearing *Myc*Tg mice is summarized in *SI Appendix*, Table S1. To further confirm whether the neoplasms were derived from a single malignantly transformed cell, we detected the *TCRβ* rearrangements by PCR amplification.

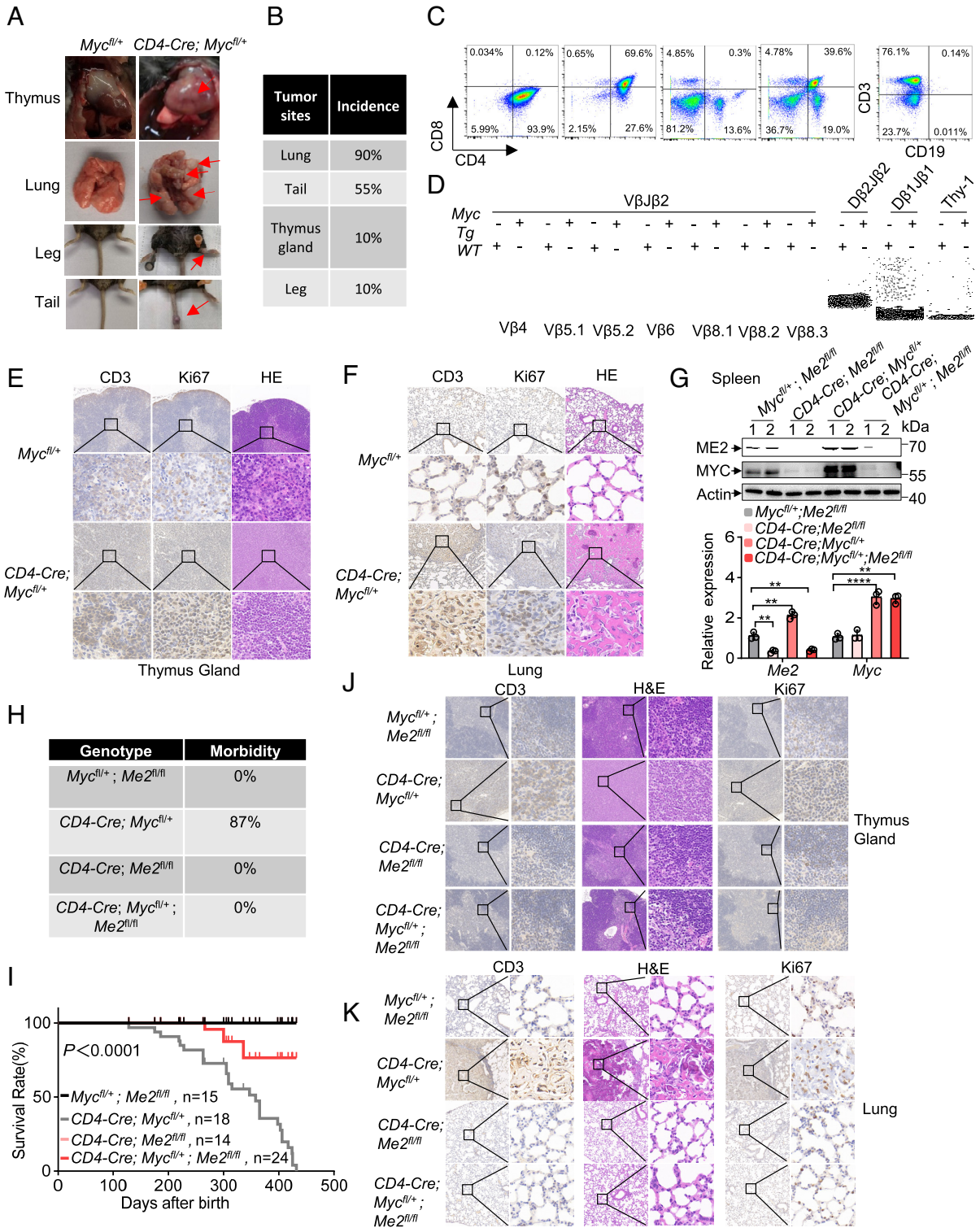

Fig. 3. *ME2* deletion prevents MYC-induced T cell lymphomagenesis in vivo. (*A*) Morphology of T cell lymphomas in thymuses, lungs, legs, and tails from *CD4-Cre; Myc*$^{fl/+}$ transgenic mice compared with the corresponding sites of *Myc*$^{fl/+}$ mice. (*B*) Tumor incident in different organs of mice. (*C*) Distributions of T cell lymphoma populations from *CD4-Cre; Myc*$^{fl/+}$ transgenic mice were determined by flow cytometry analysis with CD4, CD8, CD3, and CD19 staining. Representative images are shown. (*D*) PCR products obtained from genomic DNA in the tumors of *CD4-Cre;Myc*$^{fl/+}$ transgenic mice (Tg) or normal lymphoid tissues of control mice (WT). *Vβ-Dβ1-Jβ1* gene arrangement and *Vβ-Dβ2-Jβ2* gene arrangement were detected. *Thy-1* product was used as an internal control. (*E* and *F*) Representative images of paraffin sections analyzed by H&E or IHC as indicated. Tissues shown are normal thymus glands (*E*) or lungs (*F*) in *Myc*$^{fl/+}$ mice and thymus tumors (*E*) or lung tumors (*F*) in *CD4-Cre; Myc*$^{fl/+}$ mice. Images were captured at 10× (*Top*) and 73× (*Bottom*) magnification, respectively. (*G*) Protein (*Top*) and mRNA (*Bottom*) levels of ME2 and MYC in spleen tissues from age-matched *Myc*$^{fl/+}$; *Me2*$^{fl/fl}$*CD4-Cre; Myc*$^{fl/+}$*CD4-Cre; Me2*$^{fl/fl}$*and CD4-Cre; Myc*$^{fl/+}$*; Me2*$^{fl/fl}$ transgenic mice. (*H*) Morbidity of *Myc*$^{fl/+}$; *Me2*$^{fl/fl}$*CD4-Cre; Me2*$^{fl/fl}$*, CD4-Cre; Myc*$^{fl/+}$*, and CD4-Cre; Myc*$^{fl/+}$*; Me2*$^{fl/fl}$ transgenic mice before 6 mo. (*I*) Kaplan–Meier survival curves of transgenic mice as indicated. (*J* and *K*) Representative images of paraffin sections analyzed by H&E or IHC as indicated. Tissues shown are thymus glands (*J*) and lungs (*K*) from age-matched *Myc*$^{fl/+}$; *Me2*$^{fl/fl}$*CD4-Cre; Myc*$^{fl/+}$*, CD4-Cre; Me2*$^{fl/fl}$and *CD4-Cre; Myc*$^{fl/+}$*Me2*$^{fl/fl}$ transgenic mice. Images were captured at 10× (*Left*) and 73× (*Right*) magnification, respectively. Data in (*G*) are from n = 3 biological replicates. Data in *I* are from n = 14 to 24 biological replicates. Data are the mean ± SD. For *I*, statistical significance was calculated using log-rank analysis. Statistical significance was determined by two-tailed unpaired *t* test. Western blots are representative of three independent experiments. $^{**}P < 0.01$; $^{****}P < 0.0001$.

The *TCRβ* chains of the tumors displayed a strong distribution of restriction-variant fragments, suggesting that the tumors originated from a clonal expansion of the cells (Fig. 3*D*). Moreover, immunohistochemical (IHC) analysis of thymuses and lungs in *Myc*Tg mice exhibited positive staining for proliferation marker Ki67, as well as CD3 antigen indicating that the neoplasms originated from the T cell lineage (Fig. 3 *E* and *F*). Furthermore, hematoxylin and eosin (H&E) staining of thymic sections derived from tumor-burdened *Myc*Tg mice exhibited a complete loss of cortico-medullary structure, revealing obvious tumor mass on the lungs, with large nuclei with marginated chromatic and prominent nucleoli (Fig. 3 *E* and *F*). These data indicate that *Myc*Tg mice induce T cell lymphomagenesis, but not T cell lymphocytic leukemia.

Next, we examined whether ME2 is required for MYC-driven T cell lymphomagenesis. We generated *CD4-Cre; Me2*$^{flox/flox}$ (*Me2*KO) mice to specifically knockout *Me2* in T-lineage cells. As shown in *SI Appendix*, Fig. S5 *E* and *F*, *Me2* knockout had no effect on T cell development. To explore the role of ME2 in MYC-induced TCL tumorigenesis, we established *CD4-Cre; Myc*$^{flox/+}$*;Me2*$^{flox/flox}$ mice (*Me2*KO, *Myc*Tg mice) by mating C*D4-Cre; Me2*$^{flox/flox}$mice with *Myc*$^{flox/+}$mice (*SI Appendix*, Fig. S6*A*). The genotypes of mice were confirmed by PCR (*SI Appendix*, Fig. S6*B*). Additionally, the expression of *Myc* and *Me2* in spleen and thymus tissues was also determined by western blot and qPCR experiments (Fig. 3*G* and *SI Appendix*, Fig. S6*C*). The mice were followed from birth. Eighty-seven percent of *Myc*Tg mice manifested symptoms such as labored breath and hunched posture and exhibited neoplasms on the body surface approximately within 6 mo after birth, while the other three groups of mice remained healthy (Fig. 3*H*). *Myc*Tg mice all died by 432 d, while only 3 of the 24 mice died without clinical signs of T cell lymphoma when ablated *Me2* in *Myc*Tg mice (Fig. 3*I*). Consistent with previous findings, histological analysis of *Myc*Tg mice showed evidence of malignant lymphoma, including loss of the normal thymic cortico-medullary junction by diffuse sheets of lymphocytes with large nuclei (Fig. 3*J*). In addition, Ki67 staining showed the accelerated proliferation of malignant lymphoma cells in *Myc*Tg mice (Fig. 3*J*). Notably, knockout of *Me2* in *Myc*Tg mice completely inhibited the T cell lymphogenesis (Fig. 3*J*). Similarly, knockout of *Me2* completely suppressed the lymphoma development in lung tissues of *Myc*Tg mice (Fig. 3*K*). Nevertheless, flow cytometric analysis of bone marrow and peripheral T cells of these mice revealed that the distribution of T cell subpopulations was similar between these four groups of mice (*SI Appendix*, Fig. S6*D*). Bone marrow smear and blood smear exhibited normal white cell counts (*SI Appendix*, Fig. S6*E*). These data indicate that ME2 is essential for MYC-driven T cell lymphomagenesis in vivo.

ME2 Maintains Cellular Redox Homeostasis during MYC-Driven T Cell Lymphomagenesis. We next investigated the mechanisms by which ME2 plays the critical role in MYC-driven T cell lymphomagenesis. Our previous study reported that ME2 has a key role in glutamine metabolism (21). Consistently, silencing of *ME2* reduced glutamine consumption in Jurkat cells (Fig. 4 *A*, *Left*), but had no effect on glucose consumption (Fig. 4 *A*, *Right*). By contrast, overexpression of *ME2* enhanced glutamine consumption and restored glutamine consumption in *MYC* knockdown cells (Fig. 4 *B*, *Left*). Whereas, *ME2* overexpression did not influence glucose consumption in both control and *MYC* knockdown cells (Fig. 4 *B*, *Right*). Seahorse FuelFlex assays further showed that depletion of *ME2* or *MYC* reduced dependence of Jurkat cells on glutamine, but not on glucose (*SI Appendix*, Fig. S7 *A* and *B*). Oxygen consumption rate (OCR) measured by the Mito stress tests showed that neither *MYC* nor *ME2* knockdown affected the mitochondrial function of Jurkat cells (*SI Appendix*, Fig. S7 *C* and *D*). We extended this analysis by conducting [U-$^{13}C_5$] glutamine metabolic flux to assess the rate of glutaminolysis. Depletion of *MYC* slowed down glutaminolytic flux through malic enzymes, while enforced expression of ME2 restored this (Fig. 4 *C* and *D*). We further analyzed the function of ME2 on MYC-mediated glutamine metabolism via glutamine oxidation and reductive carboxylation (31). Knockdown of *MYC* led to reduced levels of m+4 succinate, fumarate, malate, and m+3 pyruvate, while ME2 overexpression reversed this effect (*SI Appendix*, Fig. S7*E*). Nevertheless, neither *MYC* depletion nor *ME2* overexpression affected the levels of m+5 citrate, m+2 Ac-CoA, and m+3 aspartate (*SI Appendix*, Fig. S7*F*), suggesting that MYC and ME2 affect glutamine oxidation but not reductive carboxylation in Jurkat cells. Furthermore, we performed 1,2-^{13}C glucose–tracing experiment (26, 31). Consistent with the results for glucose consumption, neither *MYC* knockdown nor *ME2* overexpression affected glucose metabolism through glycolysis or pentose phosphate pathway in Jurkat cells (Fig. 4*E* and *SI Appendix*, Fig. S7 *G* and *H*). In line with this observation, a Seahorse glycolytic rate assay further confirmed that neither *MYC* nor *ME2* affected the rate of glycolysis in Jurkat cells (*SI Appendix*, Fig. S7 *I* and *J*). Taken together, these results indicate that glutamine is the major nutrient for the growth of MYC/ME2-driven TCL.

We next investigated the role of MYC and ME2 in the adaptation of T-lymphoma cells to glutamine or glucose depletion. A significant proportion of Jurkat cells underwent cell death when cells were grown in glutamine-free medium rather than glucose-free medium, while *MYC* knockdown increased the resistance of cells to glutamine starvation (*SI Appendix*, Fig. S8 *A* and *B*). Interestingly, depletion of *ME2* also increased cells resistance to glutamine starvation (*SI Appendix*, Fig. S8 *C* and *D*). Consistent with the findings that neither *ME2* nor *MYC* affect glucose metabolism in TCL cells, glucose depletion had minimal effect on TCL cell survival (*SI Appendix*, Fig. S8 *A–D*). Taken together, these results suggest that the growth of TCL is glutamine dependent and that both MYC and ME2 play a crucial role in glutamine metabolism in TCL cells.

Glutamine is required for maintenance of redox homeostasis by producing NADPH and reduced glutathione in many cancer cells (32). Similarly, we found that glutamine depletion led to the accumulation of reactive oxygen species (ROS) levels in Jurkat cells (Fig. 4 *F* and *G*). Overexpression of *ME2* reduced the levels of ROS when cells were cultured in medium containing glutamine (Fig. 4*F*). Conversely, knockdown of *ME2* increased ROS levels (Fig. 4*G*). Notably, *MYC* knockdown rose ROS levels, while ME2 overexpression reversed it (Fig. 4*H*). Moreover, GSH levels and NADPH levels were decreased in *ME2* knockdown cells compared with control cells (Fig. 4 *I* and *J*). In contrast, overexpression of *ME2* increased the levels of GSH and NADPH and rescued them in *MYC* knockdown cells (Fig. 4 *K* and *L*). We next extended our analysis into animals. GSH levels were increased in the spleen and thymus tissues of *Myc*Tg mice compared to control mice, while *Me2* knockout reversed it (Fig. 4*M*). Similar results were observed in NADPH levels (Fig. 4*N*). Correspondingly, ROS levels were decreased in the spleen and thymus tissues of *Myc*Tg mice compared with control mice, while *Me2* knockout increased the accumulation of ROS levels in both control and *Myc*Tg mice (Fig. 4*O*). Next, we further determined the species of intracellular ROS including the superoxide radical anion (O2•–), hydroxyl radical (•OH), peroxynitrite ($ONOO^-$), and hypochlorous acid (HOCl) (33–35). Knockdown of *ME2* led to an increase in intracellular superoxide levels, but not the other species of ROS (*SI Appendix*,

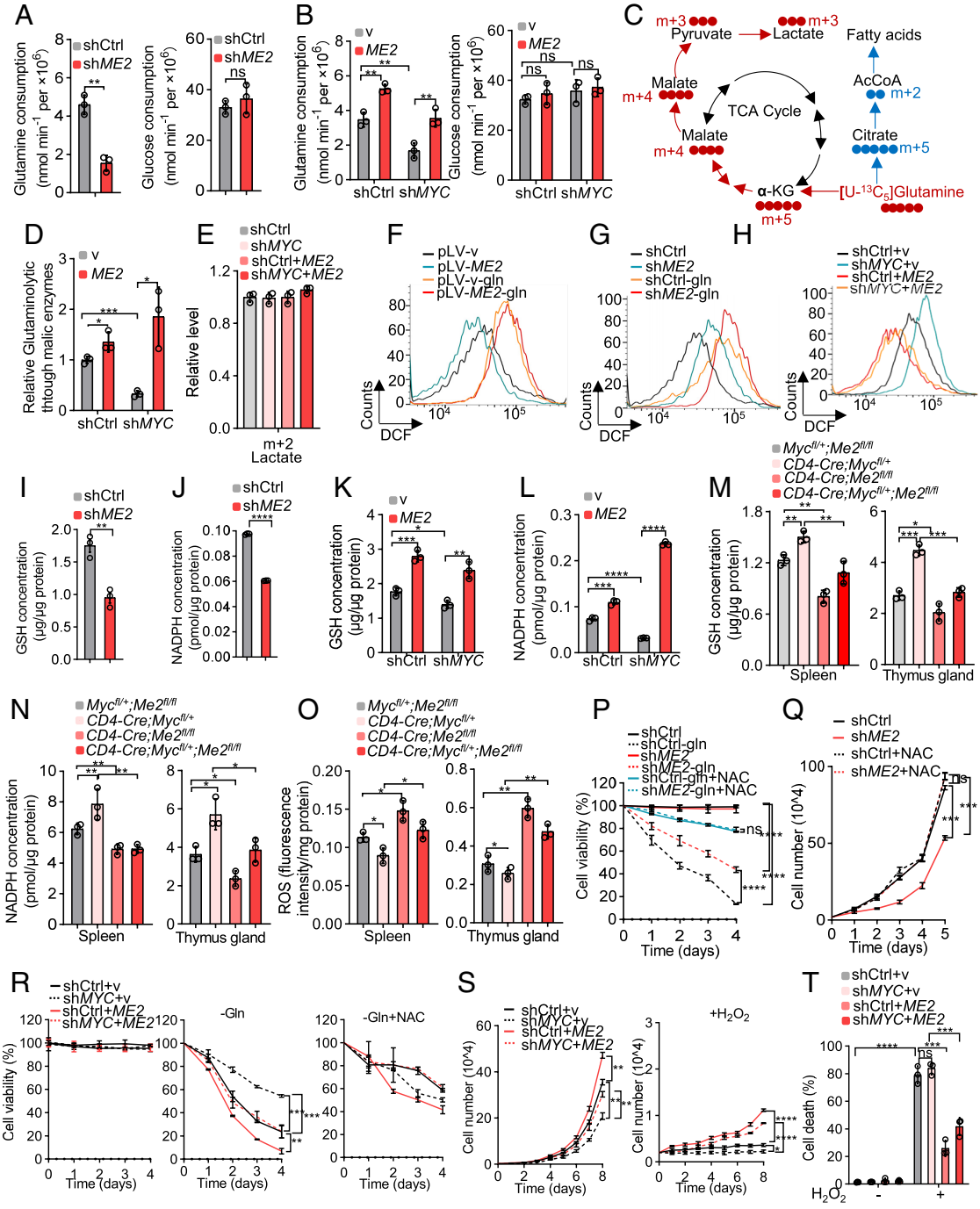

Fig. 4. ME2 maintains cellular redox homeostasis during MYC-driven T cell lymphomagenesis. (*A*) Jurkat cells stably expressing control or *ME2* shRNA were cultured for 24 h. Glutamine uptake (*Left*) and glucose uptake (*Right*) were examined. (*B*) Jurkat cells were infected with lentiviruses expressing pLKO.1-shControl (shCtrl), pLKO.1-sh*MYC* (sh*MYC*), pLKO.1-shControl-*ME2* (shCtrl+*ME2*), or pLKO.1-sh*MYC*-*ME2* (sh*MYC*+*ME2*). Glutamine uptake (*Left*) and glucose uptake (*Right*) were examined. (*C*) Schematic metabolic flux exhibiting carbon-13 (^{13}C) transfer is shown. ^{13}C transferred from [U-$^{13}C_5$] glutamine is marked as red or blue. (*D* and *E*) Jurkat cells were infected with lentiviruses expressing pLKO.1-shControl (shCtrl), pLKO.1-sh*MYC* (sh*MYC*), pLKO.1-shControl-*ME2* (shCtrl+*ME2*), or pLKO.1-sh*MYC*-*ME2* (sh*MYC*+*ME2*). Cells were cultured in medium containing [U-$^{13}C_5$] glutamine (*D*) or [1,2-^{13}C] glucose (*E*) for 12 h. ^{13}C-labeled metabolites were determined with LC–MS/MS. (*F* and *G*) Jurkat cells stably overexpressing *ME2* cDNA (*F*) or *ME2* shRNA (*G*) were cultured in the presence or absence of glutamine. ROS was examined with DCFH-DA. Gln, glutamine. (*H*) Jurkat cells were infected with lentiviruses expressing pLKO.1-shControl (shCtrl), pLKO.1-sh*MYC* (sh*MYC*), pLKO.1-shControl-*ME2* (shCtrl+*ME2*), or pLKO.1-sh*MYC*-*ME2* (sh*MYC*+*ME2*). ROS was examined with DCFH-DA. (*I* and *J*) Jurkat cells were infected with lentiviruses expressing control or *ME2* shRNA. Glutathione (GSH) levels (*I*) and NADPH levels (*J*) were examined. (*K* and *L*) Jurkat cells were infected with lentiviruses expressing pLKO.1-shControl (shCtrl), pLKO.1-sh*MYC* (sh*MYC*), pLKO.1-shControl-*ME2* (shCtrl+*ME2*), or pLKO.1-sh*MYC*-*ME2* (sh*MYC*+*ME2*). GSH levels (*K*) and NADPH levels (*L*) were examined. (*M*–*O*) GSH levels (*M*), NADPH levels (*N*), and ROS levels (*O*) were measured in spleens (*Left*) and thymus glands (*Right*) of *Myc*$^{fl/+}$*; Me2*$^{fl/fl}$*CD4-Cre; Myc*$^{fl/+}$*CD4-Cre; Me2*$^{fl/fl}$*and CD4-Cre; Myc*$^{fl/+}$*; Me2*$^{fl/fl}$ transgenic mice at the age of 2 mo. (*P*) Jurkat cells stably expressing control or *ME2* shRNA were cultured in the presence or absence of glutamine. Cells cultured in glutamine-depleted medium were treated with 2 mM NAC. Cell viability was measured by CCK8 assay and was calculated by comparing the living cell numbers to total cell numbers. (*Q*) Jurkat cells stably expressing control or *ME2* shRNA were treated with or without 2 mM NAC. Cell proliferation is shown. (*R*) Jurkat cells were infected with lentiviruses expressing pLKO.1-shControl (shCtrl), pLKO.1-sh*MYC* (sh*MYC*), pLKO.1-shControl-*ME2* (shCtrl+*ME2*), or pLKO.1-sh*MYC*-*ME2* (sh*MYC*+*ME2*). Cells were cultured in the medium with or without glutamine. And cells cultured in glutamine-depleted medium were treated with 2 mM NAC. Cell viability was measured by CCK8 assay and was calculated by comparing the living cell numbers to total cell numbers. (*S* and *T*) Jurkat cells were infected with lentiviruses expressing pLKO.1-shControl (shCtrl), pLKO.1-sh*MYC* (sh*MYC*), pLKO.1-shControl-*ME2* (shCtrl+*ME2*), or pLKO.1-sh*MYC*-*ME2* (sh*MYC*+*ME2*). Cells were treated with or without 0.1 μM H_2O_2. Cell proliferation is shown (*S*). Cell death was analyzed by flow cytometry and quantified (*T*). Data in *A*, *B*, *D*, *E*, and *I*–*T* are from n = 3 biological replicates. Data are the mean ± SD. Statistical significance was determined by two-tailed unpaired *t* test. **P* < 0.05, ***P* < 0.01; ****P* < 0.001; *****P* < 0.0001; ns *P* > 0.05.

Fig. S8 *E–H*). In contrast, overexpression of *ME2* reduced the levels of superoxide, but had no effect on the other species of ROS (*SI Appendix*, Fig. S8 *I–L*). Depletion of MYC increased intracellular superoxide levels, but not the other species of ROS, while overexpression of *ME2* reversed this effect (*SI Appendix*, Fig. S8 *M–P*). Together, these data indicate that ME2 plays a key role in MYC-mediated glutamine metabolism and maintains cellular redox homeostasis through promoting glutaminolysis.

We further investigated whether the maintenance of redox homeostasis is an important function of ME2 in TCL. Treatment with ROS scavenger N-acetyl-L-cysteine (NAC) significantly suppressed the cell death observed when the cells were cultured in glutamine-deficient medium and minimized the difference between control and *ME2*-depleted cells (Fig. 4*P* and *SI Appendix*, Fig. S9*A*). In addition, we treated cells with CB839, an inhibitor of glutaminase (GLS) that coverts glutamate into α-ketoglutarate (α-KG) (36). Likewise, NAC supplementation inhibited CB839-induced cell death in *ME2* knockdown cells and especially in control cells (*SI Appendix*, Fig. S9 *B* and *C*). Consistently, NAC treatment restored the proliferation of *ME2* knockdown cells (Fig. 4*Q*). We further explored the role of ME2 in MYC-induced T-lymphoma cell growth. *MYC* knockdown cells had a significant increase in their resistance to glutamine starvation relative to control cells, while enforced expression of *ME2* sensitized these cells to glutamine levels in the medium (Fig. 4*R*). Notably, treatment with NAC increased the resistance to glutamine deprivation and suppressed cell death induced by glutamine depletion (Fig. 4*R* and *SI Appendix*, Fig. S9*D*). Similar results were obtained when we treated the cells with CB839 (*SI Appendix*, Fig. S9 *E* and *F*), suggesting the essential role of ME2 in maintaining redox balance. In keeping with this finding, overexpression of *ME2* restored the cell proliferation of *MYC*-deficient cells (Fig. 4 *S*, *Left*). Importantly, ME2-overexpressed cells were more resistant to oxidative stress induced by H_2O_2 compared to control cells (Fig. 4*S*, *Right*). Moreover, oxidative stress led to significant cell death in both control and *MYC* knockdown cells, whereas *ME2* overexpression potently reversed it (Fig. 4 *T* and *SI Appendix*, Fig. S9*G*). NAC is a widely used antioxidant, but it is nonspecific and has many other functions (33); therefore, we used superoxide dismutase (SOD) to reduce cellular superoxide levels, which catalyzes the reduction of superoxide anions to hydrogen peroxide. Similar to the results obtained with NAC treatment, treatment with SOD significantly inhibited the cell death observed when the cells were cultured in glutamine-deficient medium and minimized the difference between control and *ME2*-depleted cells (*SI Appendix*, Fig. S9*H*). Consistently, SOD treatment restored the proliferation of *ME2* knockdown cells (*SI Appendix*, Fig. S9*I*). Moreover, enforced expression of *ME2* sensitized *MYC*-depleted cells to glutamine levels in the medium, while treatment with SOD increased the resistance to glutamine deprivation and suppressed cell death induced by glutamine depletion (*SI Appendix*, Fig. S9*J*). Together, these results suggest that ME2 promotes MYC-mediated lymphoma cell growth by maintaining cellular redox homeostasis through glutamine metabolism.

ME2 Promotes MYC Translation by Stimulating mTORC1 Activity through Glutamine Metabolism. We found that *Me2* knockout resulted in reduced MYC protein levels in both the spleen and thymus tissues of mice (Fig. 3*G* and *SI Appendix*, Fig. S6*C*). Conversely, ectopic expression of ME2 led to increased protein levels of MYC in lymphoma cells (*SI Appendix*, Fig. S4 *A*, *B*, *E*, and *G*). Notably, mutant ME2 failed to impact MYC expression (*SI Appendix*, Fig. S4 *K* and *L*), suggesting that ME2 affects MYC protein levels depending on its enzymatic activity. To investigate the role of ME2 in regulating MYC protein levels, we knocked down *ME2* in Jurkat cells. *ME2* deficiency reduced MYC protein levels, but did not affect *MYC* mRNA expression (*SI Appendix*, Fig. S10*A*). Similar results were obtained when we knocked down *ME2* using two different sets of siRNAs (*SI Appendix*, Fig. S10*B*). By contrast, ectopic expression of *ME2* increased MYC protein expression, but not mRNA levels (*SI Appendix*, Fig. S10*C*). MYC is targeted for ubiquitin-dependent proteasomal degradation (37). Depletion of *ME2* still caused a reduction in MYC protein expression, even in the presence of proteasome inhibitor MG132 (*SI Appendix*, Fig. S10*D*). In addition to the proteasome degradation system, autophagy also mediates protein degradation. Knockdown of *ME2* was still able to reduce MYC protein levels when the cells were treated with autophagy inhibitor 3-MA (*SI Appendix*, Fig. S10*E*) (38). Similarly, 3-MA treatment failed to block *ME2* overexpression–induced MYC protein expression (*SI Appendix*, Fig. S10*F*). The above findings indicate that ME2 does not affect MYC degradation. We next tested whether ME2 regulates MYC protein synthesis. We performed polysome profiling to monitor protein translation. Knockdown of *ME2* mildly affected assembly of polysomes, but reduced 80S monosome expression (Fig. 5*A*). Nevertheless, the percentage of *MYC* mRNA in polysome fractions to total mRNA was significantly decreased in *ME2*-depleted cells (*SI Appendix*, Fig. S10*G*). Moreover, in the presence of cycloheximide (CHX), a translational inhibitor that anchors polysomes onto the mRNA (39), *ME2* depletion had no effect on the MYC protein turnover (*SI Appendix*, Fig. S10*H*). In addition, overexpression of *ME2* failed to induce MYC protein expression when cells were treated with CHX (*SI Appendix*, Fig. S10*I*). Therefore, these data suggest that ME2 promotes *MYC* mRNA translation.

We next investigated the underlying mechanism by which ME2 regulates *MYC* mRNA translation. It has long been recognized that mTORC1 signaling regulates mRNA translation through phosphorylating two key effectors, p70 S6 kinase 1 (S6K1) and eukaryotic initiation factor 4E-binding proteins (4E-BPs) (40). Therefore, we examined whether mTORC1 is required for ME2-induced *MYC* mRNA translation. The colocalization of mTOR and the lysosomal marker CD63 was reduced in *ME2*-depleted cells (Fig. 5*B*). Knockdown of *ME2* resulted in reduced phosphorylation of mTORC1 substrates S6K and 4EBP1, consistent with decreased protein levels of MYC (Fig.5 *C* and *D*). To exclude the off-target effect of shRNA, we performed a rescue experiment using shRNA-resistant *ME2* cDNA. Enforced expression of exogenous *ME2* rescued the expression of *ME2* and restored MYC expression, as well as the phosphorylation of S6K and 4EBP1 (Fig. 5*C*). Conversely, ME2 overexpression enhanced the phosphorylation of S6K and 4EBP1 and the MYC protein expression (*SI Appendix*, Fig. S10*J*). Furthermore, in the presence of rapamycin, an inhibitor of mTORC1, neither knockdown nor overexpression of ME2 altered the protein levels of MYC (Fig. 5*D* and *SI Appendix*, Fig. S10*J*). Consistently, MYC protein expression stayed unchanged in *ME2*-knockdown or -overexpressed cells compared to the corresponding control cells when the cells were treated with eFT226, an inhibitor of eIF4A-dependent translation (8) (*SI Appendix*, Fig. S10 *K* and *L*). These data suggest that ME2 promotes MYC protein synthesis through stimulating mTORC1 activity. Notably, mTORC1 plays an essential role in the regulation of protein synthesis; therefore, the impact of ME2 on mTORC1 activity may not be MYC specific, but rather than a nonspecific increase in the translation of presumably all available transcripts. Whether the regulation of mTORC1 activity by ME2 is an overall regulation of protein synthesis or a translational control of specific mRNAs requires further investigation.

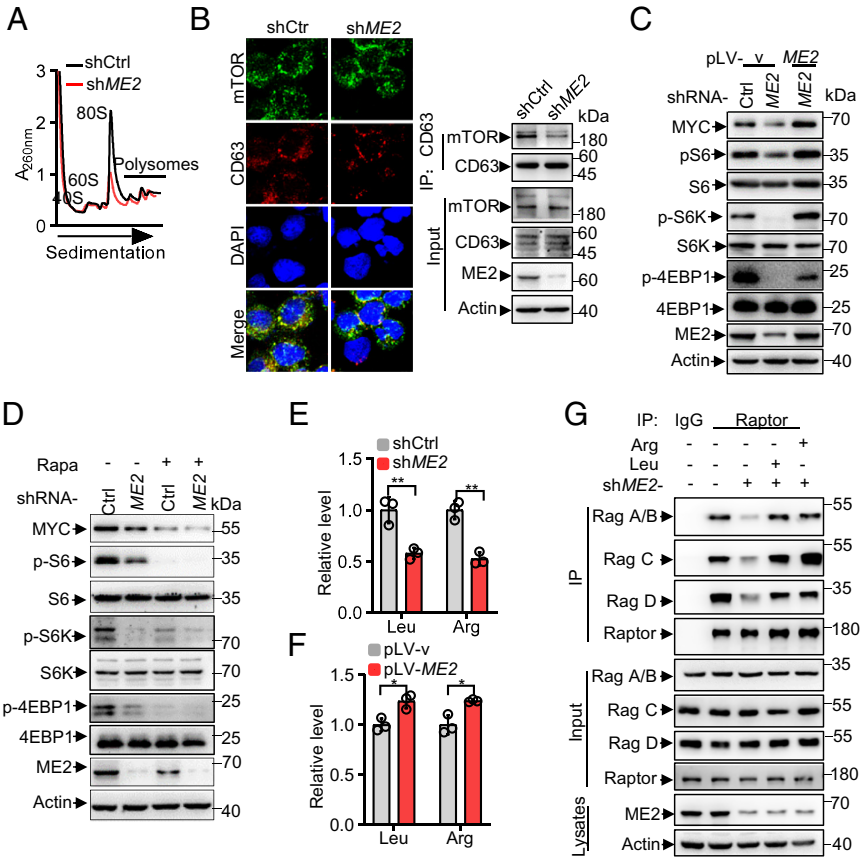

Fig. 5. ME2 promotes MYC translation through mTORC1. (*A*) Representative image of polysome profilings in Jurkat cells stably expressing *ME2* shRNA or control shRNA. (*B*) Jurkat cells were infected with lentiviruses expressing *ME2* shRNA or control shRNA. Immunofluorescence (*Left*) and co-IP (*Right*) were conducted to detect colocalization and endogenous binding of mTOR and CD63. (*C*) Jurkat cells were infected with lentiviruses expressing *ME2* shRNA or control shRNA in the presence or absence of exogenous *ME2* cDNA. Cell lysates were analyzed by western blotting for the indicated proteins and phosphorylation states. (*D*) Jurkat cells stably expressing *ME2* shRNA or control shRNA were treated with or without 500 nM rapamycin for 12 h. Cell lysates were analyzed by western blotting. Rapa, rapamycin. (*E* and *F*) Jurkat cells were infected with lentiviruses expressing *ME2* shRNA (*E*) or *ME2* cDNA (*F*). Leucine (Leu) and arginine (Arg) were examined by LC-MS. (*G*) Jurkat cells infected with lentiviruses expressing control or *ME2* shRNA were treated with 2 mM leucine (Leu) and 10 μM arginine (Arg). IP was conducted to detect endogenous binding of Raptor and Rags. Data in *E* and *F* are from n = 3 biological replicates. Data are the mean ± SD. Statistical significance was determined by two-tailed unpaired *t* test. **P* < 0.05, ***P* < 0.01.

We further examined the mechanism for the activation of mTORC1 by ME2. The activation of mTORC1 is mainly dependent on growth factors and nutrients (40). Our previous data showed that ME2 plays an important role in glutamine metabolism. Thus, we tested whether ME2 influences mTORC1 activation through altering glutamine metabolism. Deprivation of glutamine or treatment with GLS inhibitor CB839 completely eliminated the difference in MYC expression, as well as mTORC1 activity between control and *ME2* knockdown cells (*SI Appendix*, Fig. S10 *M* and *N*). Similar results were obtained when cells overexpressing *ME2* were cultured in glutamine-free medium or treated with CB839 (*SI Appendix*, Fig. S10 *O* and *P*). A wide range of signals including amino acids regulates the activity of mTORC1 (41–43). Intriguingly, we found that silencing of *ME2* reduced the levels of leucine and arginine (Fig. 5*E*). By contrast, forced expression of *ME2* resulted in elevated leucine and arginine levels (Fig. 5*F*). Furthermore, IP assays showed that depletion of *ME2* disrupted the interaction between Raptor and Rags, while supplementation with leucine or arginine reversed this effect (Fig. 5*G*). These data indicate that the activation of mTORC1 by ME2 is dependent on intracellular amino acid levels.

Rapamycin Effectively Suppresses ME2-Mediated T-Lymphoma Cell Growth. Considering the potent role for ME2 in regulating MYC translation through mTORC1, we performed both in vitro and in vivo assays to evaluate the possible inhibitory effects of rapamycin in control and ME2-overexpressing cells. We treated TCL cells with 1 nM and 500 nM rapamycin, and proliferation assay revealed a dose-dependent inhibition of cell growth (*SI Appendix*, Fig. S11*A*). Moreover, treatment with 500 nM rapamycin almost completely suppressed cell growth and anchorage-independent colony formation in control cells and especially in ME2-overexpressing cells (*SI Appendix*, Fig. S11 *A*, *Right* and *SI Appendix*, Fig. S11*B*). Interestingly, rapamycin did not induce cell apoptosis (*SI Appendix*, Fig. S11*C*).

To evaluate the role of rapamycin in tumor growth in vivo, *ME2*-overexpressing or control Jurkat cells were transplanted into NSG mice through tail vein. The mice were subsequently injected 6 mg/kg rapamycin intraperitoneally every other day (44). Consistent with previous study (44), there was no significant reduction in body weight in rapamycin-treated mice compared to untreated mice (*SI Appendix*, Fig. S11*D*). In addition, there was no significant organ injury in rapamycin-treated mice (*SI Appendix*, Fig. S11*E*). The survival time of the mice bearing *ME2*-overexpressing cells was shorter than the mice bearing control cells, while the mice treated with rapamycin survived much longer (Fig. 6*A*). Meanwhile, mice bearing *ME2*-overexpressing cells exhibited less reddish bones compared to the mice bearing control cells, while rapamycin-treated mice showed more reddish bones (Fig.6*B*). In addition, mice bearing *ME2*-overexpressing cells showed increased spleen weight (Fig. 6*C*) and more dispersion of human $CD45^+$ cells in the bone marrow, blood, and spleens (*SI Appendix*, Fig. S11*F*), and rapamycin

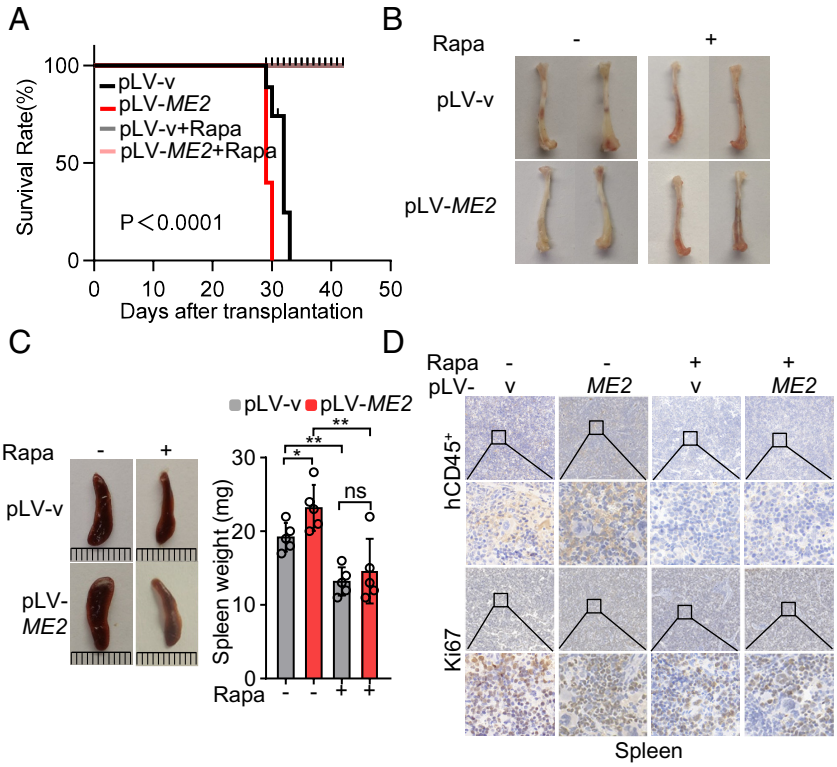

Fig. 6. Rapamycin potently suppressed ME2-induced TCL progression. (*A*–*D*) Jurkat cells overexpressing *ME2* cDNA or empty vector were transplanted into NSG mice. The mice were treated with 6 mg/kg/d rapamycin or equal amount of solvent intraperitoneally. (*A*) Kaplan–Meier survival curves of mice as indicated are shown (n = 5 biological replicates). (*B* and *C*) Representative images of thighbones (*B*) and spleens (*C*, *Left*) in four groups of NSG mice as indicated on day 28 post transplantation. Spleen weight was quantified (*C*, *Right*). (n = 5 biological replicates). (*D*) Paraffin sections of mouse spleens analyzed by immunohistochemistry with Ki67 and human CD45$^+$ staining. The spleens were obtained on day 28 post transplantation. Representative images are shown. Data in *C* are from n = 5 biological replicates. Data are the mean ± SD. Statistical significance was determined by two-tailed unpaired *t* test. For *D*, statistical significance was calculated using log-rank analysis. **P* < 0.05, ***P* < 0.01; ****P* < 0.001; *****P* < 0.0001; ns *P* > 0.05.

treatment reversed it (Fig. 6*C* and *SI Appendix*, Fig. S11*F*). Moreover, IHC staining showed a decrease in TCL burden and reduced proliferation in the spleens from rapamycin-treated mice (Fig. 6*D*). Collectively, these results suggest that inhibition of mTORC1 with rapamycin, which breaks the positive feedback loop between ME2 and MYC, can inhibit TCL progression, which may provide a therapeutic strategy for patients with TCL.

Discussion

The present study indicates that MYC promotes ME2 expression to enhance glutamine flux, thereby maintaining cellular redox homeostasis. We find that ME2 is essential for MYC-driven T cell lymphomagenesis. Malic enzymes are up-regulated in many human tumors. Interestingly, malic enzymes seem to be tightly controlled by oncogenes and tumor suppressors. For instance, our previous study reported that p53 represses the expression of all the three malic enzymes (21). In contrast, the oncogene K-Ras enhances the metabolic flux through ME1 (45). Here, we find that MYC activates ME2 expression in T cell lymphoma. These studies suggest that upregulation of malic enzymes in many human tumors, particularly ME2, may be at least partially dependent of aberrant expression of tumor suppressors or oncogenes. The general upregulation of ME2 in a wide range of human tumors suggests that human tumor cells select for the powerful and potentially ubiquitous proliferative advantage conferred by ME2.

The proto-oncogene *MYC* is one of the most frequently dysregulated oncogenes in cancer and is critical to the development of T cell malignancies (6–8). In this study, we found that heterozygous overexpression of *Myc* gene under the control of *CD4* promoter has no effect on T cell development. However, approximately 90% of the transgenic mice developed TCL within 6 mo after birth, and most of the tumors were distributed peripherally and exhibited mature immunophenotypes. TCL is relatively rare, usually clinically aggressive, and quite heterogeneous (1). Accordingly, TCL is typically associated with limited treatment options. Our work provides a spontaneous TCL mouse model and clarifies the essential role of MYC in this disease. More importantly, *Myc*Tg mice completely abolished tumorigenesis when depleted *Me2* in T cells. Although MYC regulates a wide range of tumor progression through its different target genes, our work demonstrates the critical role of ME2 as a MYC target gene in the development of MYC-driven TCL.

Glutamine deprivation impairs activation-induced T cell growth and proliferation, implicating that glutamine is an important source of biosynthetic precursors in activated T cells (46, 47). MYC plays a central role in glutamine addiction. Studies in human cell lines have suggested that enforced expression of MYC regulates the rate-limiting glutaminolytic enzyme glutaminase 1 (Gls1) through both transcriptional and posttranscriptional mechanisms (48). In this study, we find that ME2 confers MYC-mediated glutamine addiction in TCL cells. By stimulating ME2, MYC enhances cellular glutamine metabolism and promotes TCL progression. Notably, ME2 overexpressed in TCL cells maintains cellular redox homeostasis through promoting glutaminolysis. By contrast, inhibition of ME2 or glutamine metabolism sensitizes TCL cells to oxidative stress. Likewise, a recent study reported that ME1 is regulated by nuclear factor erythroid 2–related factor (NRF2) and counteracts oxidative stress in HCC (49). Together, these works suggest that malic enzymes are critical for redox balance in cancer cells.

In addition, the reciprocal regulation between MYC and ME2 may also account for the importance of ME2 in T cell lymphoma. This positive feedback loop ultimately maintains constitutively high expression of MYC and ME2 while constitutively relieving the stress of high MYC expression and ultimately promoting tumorigenesis. Therefore, breaking the MYC–ME2 axis may be an alternative therapeutic strategy for patients with TCL. Indeed, treatment with rapamycin, an inhibitor of the mTORC1 pathway, significantly reduced TCL progression both in vivo and in vitro. Our study may provide a previously unappreciated mechanism for the therapeutical effect of mTORC1 in the MYC-driven TCL treatment. However, this study used a leukemia development model in NSG mice to test the efficacy of rapamycin. To better evaluate the translational potential in TCL, rapamycin efficacy should be tested in a *Myc*Tg mouse model, as this mouse model best recapitulates human TCL disease.

Collectively, our data reveal an unexpected dependence of glutamine metabolism on ME2 during MYC-driven T cell lymphomagenesis. Given the importance of malic enzymes in maintaining redox homeostasis in cancer cells, these findings may have implications for future therapeutic approaches, as inhibition of ME2 in TCL has the potential to act synergistically with therapies that increase intracellular ROS, such as chemotherapy and radiotherapy. Moreover, the feedback regulation of ME2 on MYC underlines its importance in T cell lymphomagenesis and its potential as a therapeutic target.

Materials and Methods

Statistical Analysis. Experiments were repeated at least three times with similar results. Meanwhile, experiments were set at no less than three samples per group. *P* values were calculated using Student's two-tailed unpaired *t* test. The analysis of Kaplan–Meier survival curves were determined by log-rank analysis. Error bars represent SD between experimental replicates (mean ± SD). *P* values are provided in the figure labels, while the number of replicates is indicated in figure legends. *P* values below 0.05 were considered statistically significant. Statistics were calculated and depicted with GraphPad Prism 8.0 (GraphPad Software).

Additional methods can be found in *SI Appendix, Material and Methods*.

Data, Materials, and Software Availability. All study data are included in the article and/or *SI Appendix*.

ACKNOWLEDGMENTS. We thank Prof. Lin Wang for helping with the LC–MS/MS experiments. This work was supported by National Key Research and Development Program of China (2019YFA0802600, 2022YFA0806302), National Natural Science Foundation of China (81672766), Chinese Academy of Medical Sciences Innovation Fund for Medical Sciences (2021-I2M-1-016), Haihe Laboratory of Cell Ecosystem Innovation Fund (22HHXBSS00011), Chinese Academy of Medical Sciences Basic Research Fund (2019-RC-HL-007), and State Key Laboratory Special Fund (2060204) to W.D.

1. J. Iqbal *et al.*, Gene expression signatures delineate biological and prognostic subgroups in peripheral T-cell lymphoma. *Blood* **123**, 2915–2923 (2014).
2. C. Agostinelli *et al.*, Peripheral T cell lymphoma, not otherwise specified: The stuff of genes, dreams and therapies. *J. Clin. Pathol.* **61**, 1160–1167 (2008).
3. S. M. Horwitz *et al.*, NCCN guidelines insights: Non-Hodgkin's lymphomas, version 3.2016. *J. Natl. Compr. Canc. Netw.* **14**, 1067–1079 (2016).
4. E. D. Hsi *et al.*, Diagnostic accuracy of a defined immunophenotypic and molecular genetic approach for peripheral T/NK-cell lymphomas. A North American PTCL study group project. *Am. J. Surg. Pathol.* **38**, 768–775 (2014).
5. C. V. Dang, MYC on the path to cancer. *Cell* **149**, 22–35 (2012).
6. R. Beroukhim *et al.*, The landscape of somatic copy-number alteration across human cancers. *Nature* **463**, 899–905 (2010).
7. L. Belver, A. Ferrando, The genetics and mechanisms of T cell acute lymphoblastic leukaemia. *Nat. Rev. Cancer* **16**, 494–507 (2016).
8. A. Sabò *et al.*, Selective transcriptional regulation by Myc in cellular growth control and lymphomagenesis. *Nature* **511**, 488–492 (2014).
9. K. M. Chisholm *et al.*, Expression profiles of MYC protein and MYC gene rearrangement in lymphomas. *Am. J. Surg. Pathol.* **39**, 294–303 (2015).
10. R. Manso *et al.*, C-MYC is related to GATA3 expression and associated with poor prognosis in nodal peripheral T-cell lymphomas. *Haematologica* **101**, e336-8 (2016).
11. Y. Gu *et al.*, Stabilization of the c-Myc protein by CAMKIIγ promotes T cell lymphoma. *Cancer Cell* **32**, 115–128.e7 (2017).
12. J. M. Adams *et al.*, The c-myc oncogene driven by immunoglobulin enhancers induces lymphoid malignancy in transgenic mice. *Nature* **318**, 533–538 (1985).
13. D. W. Felsher, J. M. Bishop, Reversible tumorigenesis by MYC in hematopoietic lineages. *Mol. Cell* **4**, 199–207 (1999).
14. K. Blyth *et al.*, Sensitivity to myc-induced apoptosis is retained in spontaneous and transplanted lymphomas of CD2-mycER mice. *Oncogene* **19**, 773–782 (2000).
15. D. M. Langenau *et al.*, Cre/lox-regulated transgenic zebrafish model with conditional myc-induced T cell acute lymphoblastic leukemia. *Proc. Natl. Acad. Sci. U.S.A.* **102**, 6068–6073 (2005).
16. B. King *et al.*, The ubiquitin ligase FBXW7 modulates leukemia-initiating cell activity by regulating MYC stability. *Cell* **153**, 1552–1566 (2013).
17. R. Y. Hsu, Pigeon liver malic enzyme. *Mol. Cell. Biochem.* **43**, 3–26 (1982).
18. G. G. Chang, L. Tong, Structure and function of malic enzymes, a new class of oxidative decarboxylases. *Biochemistry* **42**, 12721–12733 (2003).
19. R. L. Pongratz, R. G. Kibbey, G. I. Shulman, G. W. Cline, Cytosolic and mitochondrial malic enzyme isoforms differentially control insulin secretion. *J. Biol. Chem.* **282**, 200–207 (2007).
20. L. Liu, S. Shah, J. Fan, J. O. Park, Malic enzyme tracers reveal hypoxia-induced switch in adipocyte NADPH pathway usage. *Nat. Chem. Biol.* **12**, 345–352 (2016).
21. P. Jiang, W. Du, A. Mancuso, K. E. Wellen, X. Yang, Reciprocal regulation of p53 and malic enzymes modulates metabolism and senescence. *Nature* **493**, 689–693 (2013).
22. W. Li *et al.*, NADPH levels affect cellular epigenetic state by inhibiting HDAC3-Ncor complex. *Nat. Metab.* **3**, 75–89 (2021).
23. W. C. Lee, X. Ji, I. Nissim, F. Long, Malic enzyme couples mitochondria with aerobic glycolysis in osteoblasts. *Cell Rep.* **32**, 108108 (2020).
24. Y. P. Wang *et al.*, Malic enzyme 2 connects the Krebs cycle intermediate fumarate to mitochondrial biogenesis. *Cell Metab.* **33**, 1027–1041.e8 (2021).
25. M. Zhao *et al.*, Malic enzyme 2 maintains protein stability of mutant p53 through 2-hydroxyglutarate. *Nat. Metab.* **4**, 225–238 (2022).
26. C. B. Brashears *et al.*, Malic enzyme 1 absence in synovial sarcoma shifts antioxidant system dependence and increases sensitivity to ferroptosis induction with ACXT-3102. *Clin. Cancer Res.* **28**, 3573–3589 (2022).
27. M. Ito *et al.*, NOD/SCID/gamma(c)(null) mouse: An excellent recipient mouse model for engraftment of human cells. *Blood* **100**, 3175–3182 (2002).
28. J. Zuber *et al.*, RNAi screen identifies Brd4 as a therapeutic target in acute myeloid leukaemia. *Nature* **478**, 524–528 (2011).
29. E. M. Blackwood, R. N. Eisenman, Max: A helix-loop-helix zipper protein that forms a sequence-specific DNA-binding complex with Myc. *Science* **251**, 1211–1217 (1991).
30. J. Stone *et al.*, Definition of regions in human c-myc that are involved in transformation and nuclear localization. *Mol. Cell. Biol.* **7**, 1697–1709 (1987).
31. M. R. Antoniewicz, A guide to (13)C metabolic flux analysis for the cancer biologist. *Exp. Mol. Med.* **50**, 1–13 (2018).
32. C. Gorrini, I. S. Harris, T. W. Mak, Modulation of oxidative stress as an anticancer strategy. *Nat. Rev. Drug. Discov.* **12**, 931–947 (2013).
33. M. P. Murphy *et al.*, Guidelines for measuring reactive oxygen species and oxidative damage in cells and in vivo. *Nat. Metab.* **4**, 651–662 (2022).
34. X. Bai, Y. Huang, M. Lu, D. Yang, HKOH-1: A highly sensitive and selective fluorescent probe for detecting endogenous hydroxyl radicals in living cells. *Angew. Chem. Int. Ed. Engl.* **56**, 12873–12877 (2017).
35. J. J. Hu *et al.*, HKOCl-3: A fluorescent hypochlorous acid probe for live-cell and in vivo imaging and quantitative application in flow cytometry and a 96-well microplate assay. *Chem. Sci.* **7**, 2094–2099 (2016).
36. M. I. Gross *et al.*, Antitumor activity of the glutaminase inhibitor CB-839 in triple-negative breast cancer. *Mol. Cancer Ther.* **13**, 890–901 (2014).
37. N. Popov, C. Schülein, L. A. Jaenicke, M. Eilers, Ubiquitylation of the amino terminus of Myc by SCF(β-TrCP) antagonizes SCF(Fbw7)-mediated turnover. *Nat. Cell Biol.* **12**, 973–981 (2010).
38. S. Miller, A. Oleksy, O. Perisic, R. L. Williams, Finding a fitting shoe for Cinderella: Searching for an autophagy inhibitor. *Autophagy* **6**, 805–807 (2010).
39. T. Schneider-Poetsch *et al.*, Inhibition of eukaryotic translation elongation by cycloheximide and lactimidomycin. *Nat. Chem. Biol.* **6**, 209–217 (2010).
40. G. Y. Liu, D. M. Sabatini, mTOR at the nexus of nutrition, growth, ageing and disease. *Nat. Rev. Mol. Cell Biol.* **21**, 183–203 (2020).
41. Y. Sancak *et al.*, The Rag GTPases bind raptor and mediate amino acid signaling to mTORC1. *Science* **320**, 1496–1501 (2008).
42. L. Bar-Peled, D. M. Sabatini, Regulation of mTORC1 by amino acids. *Trends Cell Biol.* **24**, 400–406 (2014).
43. J. Kim, K. L. Guan, mTOR as a central hub of nutrient signalling and cell growth. *Nat. Cell Biol.* **21**, 63–71 (2019).
44. H. Tang *et al.*, mTORC1 promotes denervation-induced muscle atrophy through a mechanism involving the activation of FoxO and E3 ubiquitin ligases. *Sci. Signal* **7**, ra18 (2014).
45. G. Chakrabarti, Mutant KRAS associated malic enzyme 1 expression is a predictive marker for radiation therapy response in non-small cell lung cancer. *Radiat. Oncol.* **10**, 145 (2015).
46. R. Wang *et al.*, The transcription factor Myc controls metabolic reprogramming upon T lymphocyte activation. *Immunity* **35**, 871–882 (2011).
47. D. Herranz *et al.*, Metabolic reprogramming induces resistance to anti-NOTCH1 therapies in T cell acute lymphoblastic leukemia. *Nat. Med.* **21**, 1182–1189 (2015).
48. P. Gao *et al.*, c-Myc suppression of miR-23a/b enhances mitochondrial glutaminase expression and glutamine metabolism. *Nature* **458**, 762–765 (2009).
49. D. Lee *et al.*, Adaptive and constitutive activations of malic enzymes confer liver cancer multilayered protection against reactive oxygen species. *Hepatology* **74**, 776–796 (2021).